Applied Physics Letters

15 Gb/s index-coupled distributed-feedback lasers based on 1.3 μm InGaAs quantum dots

Cite as: Appl. Phys. Lett. **105**, 011103 (2014); https://doi.org/10.1063/1.4887063
Submitted: 05 June 2014 • Accepted: 24 June 2014 • Published Online: 07 July 2014

M. Stubenrauch, G. Stracke, D. Arsenijević, et al.

15 Gb/s index-coupled distributed-feedback lasers based on 1.3 μm InGaAs quantum dots

M. Stubenrauch,[1,a)] G. Stracke,[1] D. Arsenijević,[1] A. Strittmatter,[2] and D. Bimberg[1]
[1]*Institut für Festkörperphysik, Technische Universität Berlin, Hardenbergstr. 36, 10623 Berlin, Germany*
[2]*Institut für Experimentelle Physik, Otto-von-Guericke-Universität Magdeburg, Universitätsplatz 2, 39106 Magdeburg, Germany*

(Received 5 June 2014; accepted 24 June 2014; published online 7 July 2014)

The static properties and large-signal modulation capabilities of directly modulated p-doped quantum-dot distributed-feedback lasers are presented. Based on pure index gratings the devices exhibit a side-mode-suppression ratio of 58 dB and optical output powers up to 34 mW. Assisted by a broad gain spectrum, which is typical for quantum-dot material, emission wavelengths from 1290 nm to 1310 nm are covered by the transversal and longitudinal single-mode lasers fabricated from the same single wafer. Thus, these lasers are ideal devices for on-chip wavelength division multiplexing within the original-band according to the IEEE802.3ba standard. 10 Gb/s data transmission across 30 km of single mode fiber is demonstrated. The maximum error-free data rate is found to be 15 Gb/s. © *2014 AIP Publishing LLC*. [http://dx.doi.org/10.1063/1.4887063]

Distributed-feedback (DFB) lasers are key devices for modern optical data communication systems. DFB lasers provide longitudinal single mode emission with a narrow line width, making them indispensable for dense wavelength division multiplexing (WDM) systems.[1,2] DFB lasers based on quantum dots (QDs) benefit from the same unique properties already demonstrated for ridge-waveguide edge-emitting QD lasers like high temperature stability,[3,4] low feedback sensitivity,[5] low chirp,[6] and low internal losses.[7,8] Their potential for high-speed data communication under direct modulation up to 25 Gb/s by means of excited state lasing was recently shown.[9] The typical size distribution of self-organized QDs results in a wide gain spectrum that ensures a broad distribution of target emission wavelengths and a higher insensitivity to temperature or charge carrier induced gain spectrum shifts.[10] High-speed characteristics and temperature stability of the threshold current of QD lasers is improved by p-doping of the active region.[11] Within the last years, several groups[12–16] have developed alternative concepts to realize QD DFB lasers. Since QDs can degrade at high growth temperatures, induced by indium depletion, the common technique of quantum-well (QW) DFB laser fabrication using an overgrowth step was avoided by implementation of lateral metal gratings. Such laterally-loss-coupled (LLC) DFB lasers feature proper static characteristics, like side-mode suppression ratio (SMSR) up to 50 dB and slope efficiencies in the range of 0.15 W/A.[12] In Ref. 13, modulation of single DFB lasers at 10 Gb/s was demonstrated, showing a SMSR up to 55 dB and a slope efficiency of 0.14 W/A. However, loss coupling reduces the photon life time in the effective cavity. Consequently, highly reflective facets are necessary, which complicates the monolithic integration with other devices. Moreover, the span of single-mode lasing can be limited, i.e., Fabry-Perot (FP) ground- or excited-state lasing can occur by changing operation parameters. Pure index-coupling was attempted by etching the grating vertically into the deep etched ridge, but due to large waveguide losses low slope efficiencies below 0.03 W/A as well as small SMSR of 20 dB are observed for lasers driven with pulsed currents.[14] Most recently, index-coupling with buried gratings was presented, comprising two growth steps: molecular beam epitaxy (MBE) and metal organic vapor chemical deposition epitaxy (MOCVD). At moderate temperatures an AlGaAs upper cladding were grown, accepting changes in grating form and a QD photoluminescence shift to shorter wavelengths.[15] Their devices achieved 40 dB SMSR and a slope efficiency of 0.25 W/A within a limited operation range. Substituting the upper cladding by InGaP has led to improved slope efficiency of 0.30 W/A, a 45 dB SMSR, and open eyes at 10 Gb/s.[16] Index gratings with high index contrast, superseding loss-coupled metal gratings, in combination with sufficiently large modal gain render highly reflecting mirrors unnecessary. Such InAs/GaAs-based QD DFB lasers enable monolithic integration, e.g., with electro-absorption modulators (EMLs) as low cost solutions for access networks.[17] Nevertheless, the direct modulation of QD DFB lasers did not exceed bit rates of 10 Gb/s so far. In this paper, we demonstrate a p-doped index-coupled QD DFB lasers for optical data communication at 1.31 μm showing largely improved static (increase of SMSR, slope efficiency, and output power) and dynamic properties, demonstrating operation at 15 Gb/s.

The laser structure is grown on a p-type GaAs substrate by a two-step MBE and MOCVD process. The p-doped $Al_{0.35}Ga_{0.65}As$ bottom cladding and the active region are grown by MBE. The GaAs waveguide contains 15 stacked InAs QD layers, buried in an InGaAs dot-in-a-well structure (DWELL)[18,19] to achieve a photoluminescence wavelength close to 1.3 μm. To compensate the red shift of QD gain spectra during operation, the PL spectra are optimized to be 15 nm below the target lasing wavelength. For higher threshold temperature stability and faster modulation dynamics, the 33 nm strain relaxation spacer layers between the QD layers are p-doped with a density of 5×10^{17} cm^{-3}.[11,20] Next to the waveguide, a 150 nm InGaP barrier layer and a

a)mirko.stubenrauch@tu-berlin.de

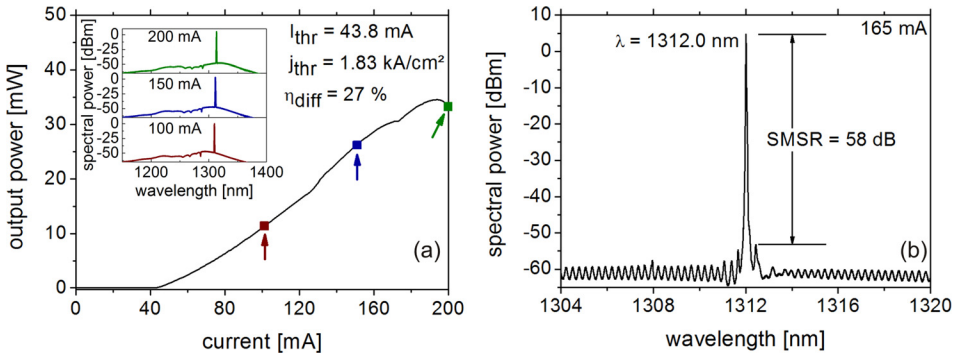

FIG. 1. Power-current characteristics of an 800 μm long QD DFB laser at room temperature (a). The inset shows the corresponding optical spectra with longitudinal single-mode emission at 100 mA, 150 mA, and 200 mA. A high-resolution optical spectrum of the DFB emission line at 165 mA (b).

100 nm GaAs DFB grating layer is grown. The barrier layer reduces the overlap of the guided mode with the grating to achieve a target coupling-length-coefficient of $\kappa L = 2$ for a 800 μm long laser, avoiding strong nonlinearity effects in the cavity, like spatial hole burning.[21] The index grating is fabricated by means of inductive-coupled plasma reactive ion etching (ICP-RIE) and electron beam lithography forming the SiNx mask. Simulations of the final structure considering the effective refraction index of the guided mode lead to grating periods of 192 nm to 195 nm for emission at O-band wavelengths. During the MOCVD growth step, the upper n-InGaP cladding and a highly n-doped GaAs contact layer are deposited. The advantages of using InGaP, instead of the more common AlGaAs upper cladding, is twofold: an increased refractive index difference to GaAs, and reduced impurity incorporation at low growth temperatures, necessary to suppress QD degradation. Due to the differences of the claddings and the resulting deformation of the guided mode we shifted the QD layers slightly away from the center of the waveguide. 3 μm wide and deep etched ridges are defined by standard photo lithography using ICP-RIE to achieve transversal single-mode operation. To reduce electrical parasitic capacitances and allow high-speed operation the structure is planarized with Benzocyclobutene and both contacts are placed on the top.[22] For ridge n-metallization Ni/AuGe/Au and for p-contacts Ni/Zn/Au are deposited in a high-speed ground-signal-ground configuration. After thinning, backside metallization, and cleaving into 800 μm long lasers, the front facet is antireflection (AR) ($R < 10^{-4}$) and the rear facet is high reflection coated ($R = 0.98$) at 1.31 nm.

For static and dynamic characterization the laser is mounted on a temperature controlled copper heat sink at 21 °C. The total optical power is determined by an integrating sphere. For spectral and dynamic measurement, the emission from the AR coated facet was coupled into a standard single-mode fiber (SMF-28). Typical static characteristics of these devices are shown in Figure 1. The power-current curve shows a threshold current of 43.8 mA corresponding to 1.83 kA/cm^2 threshold current density, and a maximum optical output power of about 34 mW. The differential quantum efficiency, derived from a linear fit between 45 mA and 180 mA, is 27%. The inset shows the corresponding lasing spectra at 100 mA, 150 mA, and 200 mA, representative for the whole current range. Longitudinal single-mode operation with suppressed excited-state emission is observed. The spectrum at 165 mA, shown in Fig. 1(b), and taken at the large-signal operation point, shows a DFB lasing mode at 1312.0 nm and a highly suppressed FP underground leading to a remarkable SMSR of 58 dB. The stop-band is not clearly visible since the structural properties (HR/AR coating, coupling factor, laser length, etc.) of the presented laser lead to a stop-band width that is in the range of the FP-mode spacing and therefore not really distinguishable. The true spectral line width is measured using a self-homodyne technique[23] and amounts to 6 MHz. The laser thus operates longitudinal and transversal (TEM_{00}) single mode.

Typical LI characteristics for temperatures from 10 °C to 55 °C are shown in Figure 2(a) with threshold currents between 38.3 mA and 49.5 mA. The reduced temperature sensitivity of threshold current is due to the p-doping of the active region. From 10 °C to 40 °C, the threshold current density is described by a negative characteristic temperature T_0 of −130 K, followed by a stable region of hardly any temperature dependence (infinite T_0) up to at least 60 °C. The thermal roll over, induced by the decrease of charge carrier population of the QD ground states, shifts to lower current with the increase of temperature. Since the QD gain has a full width at half maximum of about 80 meV, plenty of QD DFB lasers can be fabricated on the same wafer with a variety of grating periods. In Figure 2(b), four DFB lasers

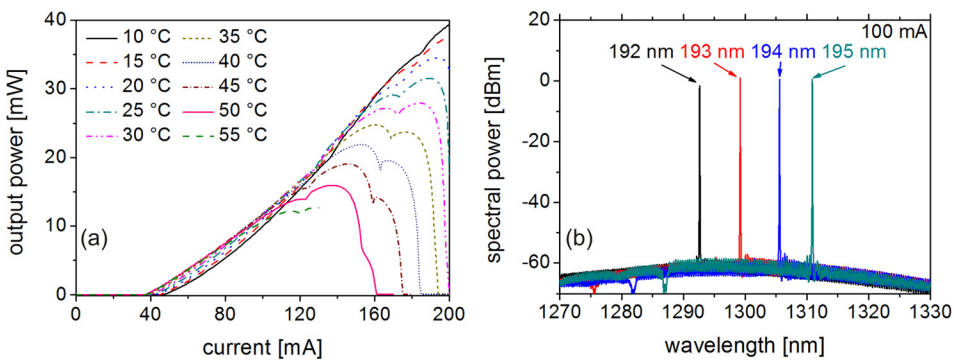

FIG. 2. Power-current characteristics for different heat sink temperatures from 10 °C to 55 °C (a). Optical spectra of four QD DFB lasers at 100 mA with different grating periods from a single wafer (b).

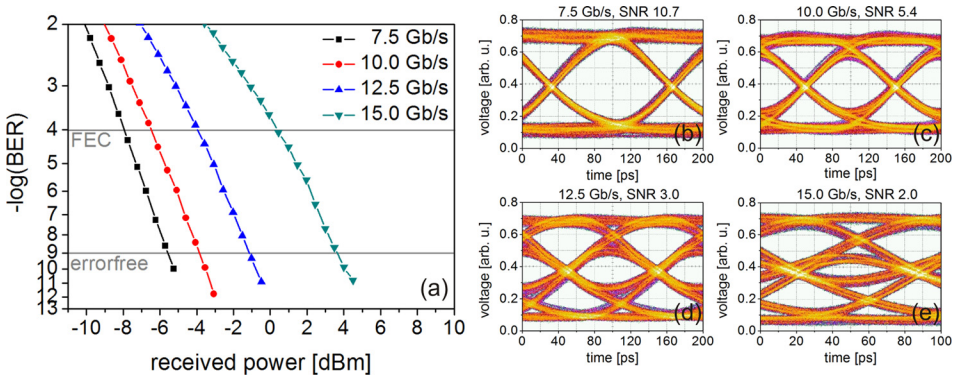

FIG. 3. Bit-error-ratio versus received optical power (a) and corresponding eye diagrams at 7.5 Gb/s (b), 10 Gb/s (c), 12.5 Gb/s (d), and 15 Gb/s (e).

showing about 58 dB SMSR with emission in the IEEE 802.3ba specification range from 1290 nm to 1310 nm are depicted as examples. From the same wafer, single-mode lasing operation can be observed for a much larger range from 1274 nm to 1336 nm (not shown here) with SMSR always larger than 30 dB.

The dynamic large-signal response under direct modulation is investigated using a non-return-to-zero (NRZ) bit pattern generator creating an electrical pseudo-random binary sequence (PRBS) on-off-keying (OOK) signal with a word length of 2^7–1 bits. The electrical signal, applied to the not 50 Ω impedance matched device, is amplified and via a bias-tee superimposed to a drive current of 165 mA. The swing amplitude is about 1.5 V. For eye diagram and bit-error ratio (BER) measurements, we used a back-to-back (B2B) configuration with direct detection. Thus, the receiver consists only of a variable optical attenuator with an optical power meter and a 50 GHz photo diode with an electrical post amplifier. For the eye diagrams, a 50 GHz sampling oscilloscope and for BER curves an error analyzer (EA) were used. B2B large-signal measurements lead to clearly open eye diagrams up to 15 Gb/s as depicted in Figure 3(b). At 15 Gb/s, 12.5 Gb/s, 10 Gb/s, and 7.5 Gb/s signal-to-noise ratios (SNR) of 2.2, 3.0, 5.4, and 10.7 are determined, respectively. For all bit rates error-free (BER below 10^{-9}) transmission is demonstrated (Figure 3(a)) without error floors. The received optical power at error-free limit are −5.5 dBm (7.5 Gb/s), −3.8 dBm (10 Gb/s), −1.1 dBm (12.5 Gb/s), and 3.6 dBm (15 Gb/s), respectively. The slight bend in BER curves at higher bit rates result from lower eye opening and relatively coarse EA threshold accuracy.

In order to proof the suitability for system applications in short-haul WDM systems BERs were recorded for different fiber lengths at 10 Gb/s (SNR of 5.4). In Figure 4, the BER curves for B2B and SMF lengths of 10 km, 20 km, and 30 km are shown. Without any kind of optical amplification error-free transmission with no visible error floor is demonstrated for at least 30 km with a negligible penalty of below 0.5 dB and corresponding received power of −4 dBm.

To summarize, we have demonstrated high-speed modulation up to 15 Gb/s of QD DFB lasers at 1.31 μm. The purely index-coupled QD DFB lasers exhibit longitudinal and transversal single mode operation up to 5 times the threshold current with a differential efficiency of 27%. The lasers show output power up to 34 mW and due to p-doping a large temperature stability with a negative characteristic temperature larger than −130 K up to 40 °C. Devices processed from a single wafer cover a wavelength range from 1290 nm to 1310 nm with a high SMSR of >58 dB. Error-free data transmission at a record 15 Gb/s at a receiver power of 3.6 dBm in direct detection mode is demonstrated. Furthermore, data transmission across 30 km of SMF without optical amplification are demonstrated.

This work was supported by the Sonderforschungsbereich 787 of the German Research Council. The authors want to thank A. Sigmund, R. Steingrüber, and M. Möhrle from the FhG Heinrich-Hertz-Institute for assistance with e-beam writing.

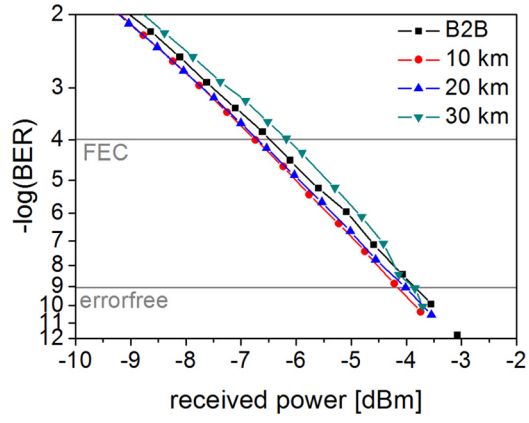

FIG. 4. Bit-error-ratio versus received optical power for 10 Gb/s direct data transmission over different fiber lengths up to 30 km.

[1]H. Ghafouri-Shiraz, "Distributed Feedback Laser Diodes and Optical Tunable Filters" (John Wiley & Sons Ltd., Chichester, 2003), Chap. 4.
[2]L. A. Coldren, S. Corzine, and M. Masanovic, "Diode Lasers and Photonic Integrated Circuits, 2nd Edition" (John Wiley & Sons, Inc., Hoboken, 2012), p. 484.
[3]R. L. Sellin, C. Ribbat, M. Grundmann, N. N. Ledentsov, and D. Bimberg, Appl. Phys. Lett. **78**, 1207 (2001).
[4]O. B. Shchekin and D. G. Deppe, Appl. Phys. Lett. **80**, 3277 (2002).
[5]D. O'Brien, S. P. Hegarty, G. Huyet, J. G. McInerney, T. Kettler, M. Laemmlin, D. Bimberg, V. M. Ustinov, A. E. Zhukov, S. S. Mikhrin, and A. R. Kovsh, Electron. Lett. **39**, 1819 (2003).
[6]D. Bimberg, N. Kirstaedter, N. N. Ledentsov, Zh. I. Alferov, P. S. Kop'ev, and V. M. Ustinov, IEEE J. Sel. Top. Quantum Electron. **3**, 196 (1997).
[7]D. Bimberg, M. Kuntz, and M. Laemmlin, Appl. Phys. A **80**, 1179 (2005).
[8]D. Bimberg, Electron. Lett. **44**, 168 (2008).
[9]D. Arsenijević, A. Schliwa, H. Schmeckebier, M. Stubenrauch, M. Spiegelberg, D. Bimberg, V. Mikhelashvili, and G. Eisenstein, Appl. Phys. Lett. **104**, 181101 (2014).

[10]D. Bimberg, M. Grundmann, N. N. Ledentsov, S. S. Ruvimov, P. Werner, U. Richter, J. Heydenreich, V. M. Ustinov, P. S. Kopev, and Z. I. Alferov, Thin Solid Films **267**, 32 (1995).
[11]D. G. Deppe, H. Huang, and O. B. Shchekin, IEEE J. Quantum Electron. **38**, 1587 (2002).
[12]H. Su and L. F. Lester, J. Phys. D: Appl. Phys. **38**, 2112 (2005).
[13]F. Gerschutz, M. Fischer, J. Koeth, M. Chacinski, R. Schatz, O. Kjebon, A. Kovsh, I. Krestnikov, and A. Forchel, Electron. Lett. **42**, 1457 (2006).
[14]K. Goshima, T. Amano, K. Akita, R. Akimoto, T. Sugaya, M. Mori, and K. Komori, Jap. J. Appl. Phys. **48**, 050203 (2009).
[15]J. J. Hu, D. Klotzkin, J. S. Huang, X. Y. Sun, and N. Y. Li, IEEE Photonics Technol. Lett. **23**, 329 (2011).
[16]K. Takada, Y. Tanaka, T. Matsumoto, M. Ekawa, H. Z. Song, Y. Nakata, M. Yamaguchi, K. Nishi, T. Yamamoto, M. Sugawara, and Y. Arakawa, Electron. Lett. **47**, 206 (2011).
[17]A. Ramdane, F. Devaux, N. Souli, D. Delprat, and A. Ougazzaden, IEEE J. Sel. Top. Quantum Electron. **2**, 326 (1996).
[18]A. R. Kovsh, A. E. Zhukov, N. A. Maleev, S. S. Mikhrin, V. M. Ustinov, A. F. Tsatsul'nikov, M. V. Maksimov, B. V. Volovik, D. A. Bedarev, Y. M. Shernyakov, E. Y. Kondrat'eva, N. N. Ledentsov, P. S. Kop'ev, Z. I. Alferov, and D. Bimberg, Semiconductors **33**, 929 (1999).
[19]A. Stintz, G. T. Liu, H. Li, L. F. Lester, and K. J. Malloy, IEEE Photonics Technol. Lett. **12**, 591 (2000).
[20]I. P. Marko, N. F. Masse, S. J. Sweeney, A. D. Andreev, A. R. Adams, N. Hatori, and M. Sugawara, Appl. Phys. Lett. **87**, 211114 (2005).
[21]H. Soda, Y. Kotaki, H. Sudo, H. Ishikawa, S. Yamakoshi, and H. Imai, IEEE J. Quantum Electron. **23**, 804 (1987).
[22]M. Kuntz, G. Fiol, M. Lämmlin, D. Bimberg, M. G. Thompson, K. T. Tan, C. Marinelli, A. Wonfor, R. Sellin, R. V. Penty, I. H. White, V. M. Ustinov, A. E. Zhukov, Yu. M. Shernyakov, A. R. Kovsh, N. N. Ledentsov, C. Schubert, and V. Marembert, New J. Phys. **6**, 181 (2004).
[23]T. Okoshi, K. Kikuchi, and A. Nakayama, Electron. Lett. **16**, 630 (1980).